Available online at www.sciencedirect.com

SciVerse ScienceDirect

Ceramics International 38 (2012) 3489–3497

CERAMICS INTERNATIONAL

www.elsevier.com/locate/ceramint

Degradation behavior against surge stress of Zn–Pr–Co–Cr–Y–Er varistor ceramics modified with Er_2O_3

Choon-W. Nahm *

Semiconductor Ceramics Laboratory, Department of Electrical Engineering, Dongeui University, Busan 614-714, Republic of Korea

Received 4 November 2011; received in revised form 20 December 2011; accepted 20 December 2011
Available online 31 December 2011

Abstract

The degradation behavior against a surge-current in the ZPCCYE ($ZnO–Pr_6O_{11}–CoO–Cr_2O_3–Y_2O_3–Er_2O_3$) varistors was investigated for different amounts of Er_2O_3. The addition of Er_2O_3 has a significant effect on nonlinear electrical properties and surge degradation behavior of the ZPCCYE varistors. Increasing amount of Er_2O_3 improved the clamp characteristics, in which the clamping voltage (K) decreases at a surge-current of 1–40 A. The varistors added with 0.5 mol% Er_2O_3 exhibited the strongest electrical stability, with the variation rate of the breakdown field of −3.2%, the variation rate of the nonlinear coefficient of −20.9%, and the variation rate of the leakage current of −40.0% after applying 1000 times for a surge-current of 100 A/cm^2. Furthermore, the varistors added with 0.5 mol% Er_2O_3 exhibited the good surge withstand capability with the variation rate of the breakdown field of −7.9% after applying the surge-current of 400 A. On the contrary, the varistors added with 0.25 mol% were destroyed after applying the surge-current of 400 A and the varistors added with 1.0 mol% were destroyed after applying 55 times for a surge-current of 100 A/cm^2.

Keywords: Surge-current; Surge degradation behavior; Clamp voltage ratio; ZPCCYE Varistors

1. Introduction

In recent, the electronic systems combined with semiconductors have migrated towards the manufacture of increased density circuits, with the same capability obtainable in a smaller package or increased capability in the same package [1]. This results in a greater susceptibility to various surges, such as transient over-voltage and electrostatic discharge (ESD). Therefore, the electronic devices sensitive to various surges should be protected by any means.

The zinc oxide (ZnO) varistors are semiconducting solid-state electronic devices formed by sintering zinc oxide with a primary (bismuth, praseodymium, and vanadium) and subordinate additives (cobalt, manganese, chromium, etc.). They are switching devices acting with the level of voltage whose resistance decreases drastically when voltage is increased up to threshold voltage, called varistor voltage. They possess excellent surge withstand capability because ZnO varistors are multi-junction devices, which consisted of the microstructure of semiconducting ZnO grain-insulating intergranular layer-semiconducting ZnO grain, unlike Zener diode of single junction [2,3]. The zinc oxide varistors have been used extensively in the field of circuit overvoltage protection, with application ranging from a few volts in electronic circuits to millions of volts in electric power systems [3–5].

Most investigations for $ZnO–Pr_6O_{11}$-based varistors have been reported on the microstructure and electrical properties in terms of additives and sintering process [4–12]. In particular, Nahm et al. reported the effect of rare earth oxides and lanthanum oxide on electrical properties and its stability against DC accelerated degradation stress [13–19]. In an application of varistors, important factors that should be considered in the application are the nonlinearity and its stability, and surge withstand capability (SWC). The electronic equipments and the electrical power systems to be protected from various surges significantly demand a high stability of varistors in order to enhance reliability. Therefore, the electrical stability against a surge-current is technologically very important in zinc oxide varistors [18–24]. Our previous work, the pulse aging behavior of the Pr_6O_{11}-based ZnO varistors consisting of 5 components

* Corresponding author. Tel.: +82 51 890 1669; fax: +82 51 890 1664.
E-mail address: cwnahm@deu.ac.kr.

0272-8842/$36.00
doi:10.1016/j.ceramint.2011.12.063

was investigated [22–24] and these varistor ceramics exhibited relatively lower breakdown field than the varistor ceramics to introduce. To develop varistor ceramics for high performance and diverse applications with high breakdown field, it is important to scrutinize the effects of additives and sintering process on varistor properties and aging behavior against a surge stress. In this work, the electrical properties [25] and surge degradation behavior against a surge-current of the ZPCCYE ($ZnO–Pr_6O_{11}–CoO–Cr_2O_3–Y_2O_3–Er_2O_3$) varistors was addressed.

2. Experimental procedure

2.1. Sample preparation

The samples were manufactured by the traditional standard ceramic technique. Reagent-grade raw materials with 99.9% purity were weighed in proportions of $(97.5 - x)$ ZnO + 0.5 Pr_6O_{11} + 1.0 CoO + 0.5 Cr_2O_3 + 0.5 Y_2O_3 + x Er_2O_3 (x = 0.25, 0.5, 1.0, all in mol%). Raw materials were mixed by ball milling with zirconia balls and acetone in a polypropylene bottle for 24 h. The powder mixture was dried at 120 °C for 12 h and calcined in air at 750 °C for 2 h. The calcined mixture was pulverized using an agate mortar/pestle and after 2 wt% polyvinyl alcohol (PVA) binder addition, granulated by sieving through a 100-mesh screen to produce the starting powder. The powder was pressed into discs of 10 mm in diameter and 2 mm in thickness at a pressure of 80 MPa. The discs were sintered at 1340 °C in air for 1 h, with heating and cooling rates of 4 °C/min. The sintered samples were lapped and polished to 1.0 mm thickness. The final samples were about 8 mm in diameter and 1.0 mm in thickness. Silver paste was coated by screen-printing techniques on both faces of the samples and the electrodes were formed by heating it at 600 °C for 10 min. The electrodes were 5 mm in diameter. Finally, after the lead wire is soldered to both electrodes, the samples were packaged by dipping it into a thermoplastic resin powder.

2.2. Microstructure examination

For microstructure characterization, both surfaces of the samples were lapped and ground with SiC paper and polished with 0.3 μm-Al powder to a mirror-like surface. The polished samples were thermally etched at 1050 °C for 30 min. The surface microstructure was examined by a scanning electron microscope (SEM, Hitachi S2400, Chiyoda-Ku, Tokyo, Japan). The average grain size (d) was determined by the lineal intercept method, given by $d = 1.56L/MN$, where L is the random line length on the micrograph, M is the magnification of the micrograph, and N is the number of the grain boundaries intercepted by the lines [26]. The crystalline phases were identified by an X-ray diffractometer (XRD, Rigaku D/max 2100, Shibuya-Ku, Tokyo, Japan) using a CuK_α radiation. The sintered density (ρ) was measured using a density determination kit (238490) attached to balance (AG 245, Mettler Toledo International Inc., Greifensee, Switzerland).

2.3. Electrical measurement

The relation between the electric field (E) and the current density (J) is described by the empirical law, $J = C \cdot E^\alpha$, where the C is a constant and the α is the nonlinear coefficient. The E–J characteristics were measured using a V–I source (Keithley 617, Keithley Instruments Inc., Cleveland, OH, USA). The breakdown field ($E_{1\,mA/cm^2}$) was measured at a current density of 1.0 mA/cm^2. The α was determined by the following expression, $\alpha = (\log J_2 - \log J_1)/(\log E_2 - \log E_1)$, where E_1 and E_2 are the electric fields corresponding to J_1 = 1.0 mA/cm^2 and J_2 = 10 mA/cm^2, respectively.

2.4. Clamping voltage measurement

The clamping voltage (V_c) is defined by the drop voltage between electrodes of varistor when the specified surge-current flows through varistor. The V_c was measured at the 8/20 μs surge-current (I_p) of 1, 5, 10, 20, and 40 A using a surge generator (Tae-yang Eng., Busan, Korea) and an oscilloscope (TeK 3020B, Tektronix Inc., Beaverton, OR, USA). The clamp voltage ratio ($K = V_c/V_{1\,mA}$) is defined by the ratio of clamping voltage to breakdown voltage. The breakdown voltage ($V_{1\,mA}$) was measured at a current of 1.0 mA DC.

2.5. Surge degradation stress test

The samples were subjected to the 8/20 μs surge-current stress with a current density of 100 A/cm^2 (40 A) by the following conditions: (i) The 1st applied surge-current of 100 times, (ii) The 2nd applied surge-current of 400 times, (iii) The 3rd applied surge-current of 700 times, (iv) The 4th applied surge-current of 1000 times. The time interval between the applied surge-currents was 2 s and the time interval between each surge-current cycle was 15 min. After applying the respective surge-current cycles, the V–I characteristics were measured at room temperature.

2.6. Surge withstand capability test

The surge withstand capability (SWC) was performed at the 8/20 μs surge-currents of 400 and 900 A using a surge generator. After applying the surge-current, the V–I characteristics were measured at room temperature.

3. Results and discussion

Fig. 1 shows SEM micrographs of the samples for different amounts of Er_2O_3. The average grain size (d) decreased in the order of 6.5, 5.9, and 5.6 μm with increasing amount of Er_2O_3 [25]. This is attributed to the increase of secondary phases. It is confirmed by XRD analysis, as indicated in Fig. 2 that on the surfaces, all samples reveal microstructure consisting to the Pr-rich and Er-rich intergranular layer as a minor secondary phase (whitish), in addition to a major phase of hexagonal ZnO (blackish). The sample added with more amount of Er_2O_3 generates more intergranular layers. It will be discussed how

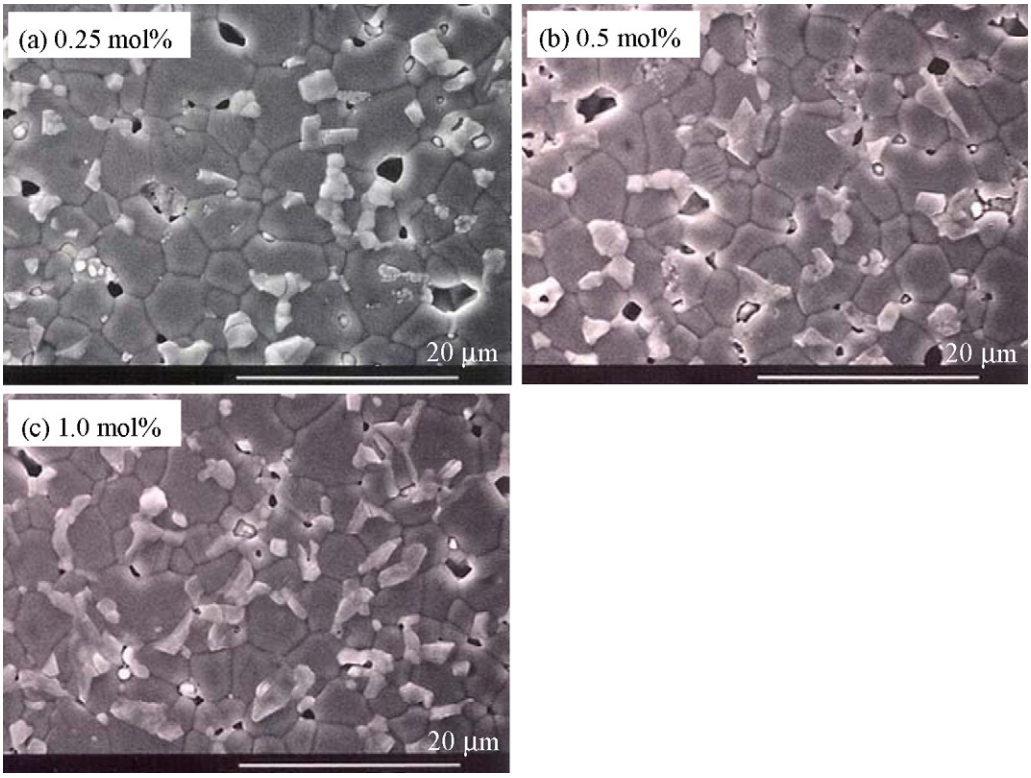

Fig. 1. SEM micrograph of the samples for different amounts of Er_2O_3.

the secondary phases will affect degradation behavior against a surge-current later. The sintered densities (ρ) of each sample exhibited 5.46, 5.40, and 5.56 g/cm^3 (theoretical density 5.78 g/cm^3 in ZnO) with increasing amount of Er_2O_3 [25].

Fig. 3 shows the *E–J* characteristics of the samples for different amounts of Er_2O_3. The *E–J* characteristics show that it acts as an ohmic resistor until the breakdown field is reached. However, thereafter, the current suddenly increases. A knee states on the curves between the two regions greatly affect nonlinear properties. The *E–J* characteristic parameters calculated from Fig. 3 are shown in Table 1. The breakdown field ($E_{1\,mA/cm^2}$) increased from 4026 to 6043 V/cm with increasing amount of Er_2O_3 [25]. The $E_{1\,mA/cm^2}$ is determined by the average grain size (d) and the breakdown voltage per grain boundary (v_{gb}), as can be seen at the following expression, $E_{1\ mA\ cm^2} = v_{gb}/d$. The increase of $E_{1\,mA/cm^2}$ can be explained by the increase in the number of grain boundaries due to the decrease of average grain size and by the increase of v_{gb}, which increases in the order of 2.6, 2.9, and 3.4 V/gb with increasing amount of Er_2O_3.

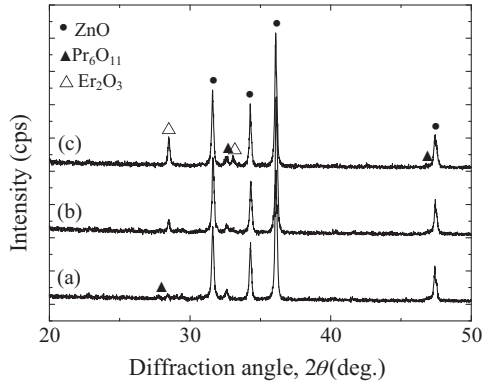

Fig. 2. XRD patterns of the samples for different amounts of Er_2O_3: (a) 0.25 mol%, (b) 0.5 mol% and (c) 1.0 mol%.

The nonlinear coefficient (α) significantly increased from 36 to 48 with increasing amount of Er_2O_3 [25]. In general, the behavior of α can be related to the variation of the Schottky barrier height according to the variation of the electronic states at the grain boundaries. The addition of Er_2O_3 may be varying the density of the interface states at the grain boundary. Therefore, the increase of α with increasing amount of Er_2O_3 is attributed to the increase of Schottky barrier height at the grain boundaries. The J_L changed in the order of 0.7, 1.5, and 0.8 μA/cm^2 with increasing amount of Er_2O_3. All the samples exhibited to have low leakage current below 0.3 μA.

If a surge withstand capability as the inherent role of varistor is low, even though the nonlinearity is good and the stability against DC accelerated aging stress is high, it is difficult to apply the varistors to the electrical and electronic fields as a surge protection device (SPD). So, a surge withstand capability is no less important than others.

Fig. 4 shows the clamping voltage (V_c) characteristics corresponding to the surge-currents of 1 and 10 A of the samples for different amounts of Er_2O_3. The higher surge-current leads to the higher V_c because the resistance in the nonlinear region exists still as a low value [20,21]. It can be seen that the higher breakdown voltage leads to the higher clamping voltage. The detailed clamping voltage (V_c) and clamp ratio (K)

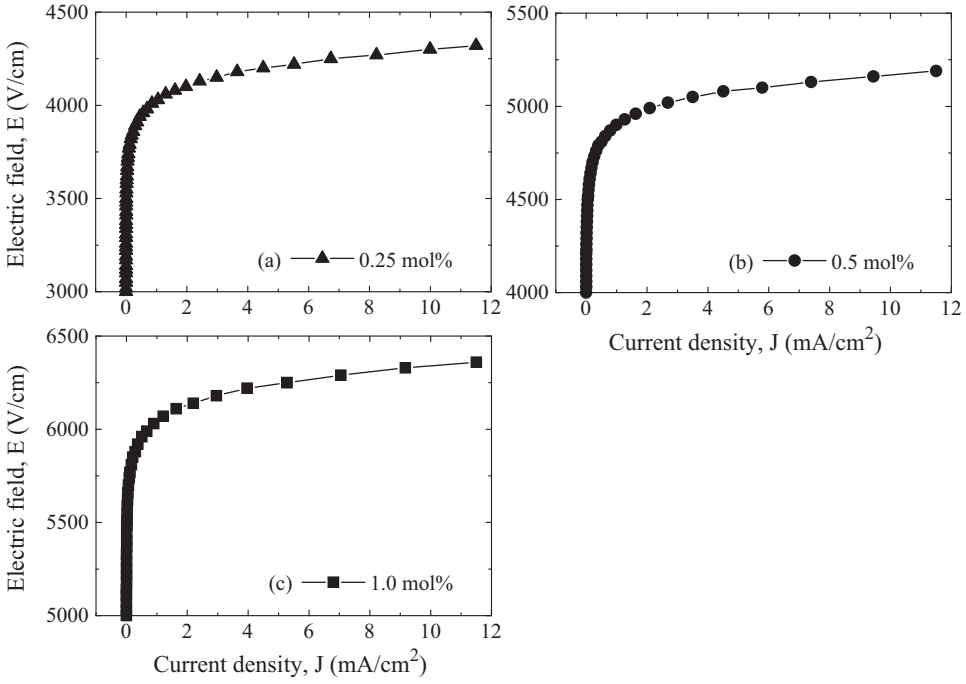

Fig. 3. *E–J* characteristics of the samples for different amounts of Er_2O_3.

against a surge-current is summarized in Table 2. The *K* value means that the varistor clamps a surge-current to a reference voltage, that is, breakdown voltage. With increasing amount of Er_2O_3, the K value decreased from 1.60 to 1.51 at a surge-current of 1 A and from 1.92 to 1.77 at a surge-current of 10 A. As a result, an increasing amount of Er_2O_3 led to lower *K* value for all surge-currents. It can be seen that Er_2O_3 has a significant effect on the clamping characteristics.

Fig. 5 is the surge-current waveforms of 100 A/cm^2 applied to the samples in order to investigate a surge degradation behavior against a surge-current stress for different amounts of Er_2O_3. Then the clamping voltage exhibited 900, 925, and 1240 V, respectively, with increasing amount of Er_2O_3. Fig. 6 compares the variation of *E–J* characteristics after applying the surge-current stress of 100 A/cm^2 with the initial *E–J* characteristics for different amounts of Er_2O_3. The samples added with 1.0 mol% Er_2O_3 were destroyed after applying 55 times and completely lost the nonlinear properties. The sample destroyed is shown in Fig. 7(a). As can be seen, a part of package chipped off by the shock of surge. The addition of Er_2O_3 will lead to many secondary phases existing at grain boundary and triple point. This results in the decrease of effective area of the grain boundary. As a result, it is assumed that this failure is attributed to very high surge-current density per grain boundary due to many secondary phases. The samples added with 0.25 and 0.5 mol% Er_2O_3 exhibited very high stability against a surge-current stress. In particular, the samples added with 0.5 mol% Er_2O_3 exhibited a smaller *E–J* characteristic variation than that of the samples added with 0.25 mol% Er_2O_3. The *E–J* characteristic parameters after applying the surge-current are compared with initial *E–J* characteristics, as shown in Table 2. After applying the surge stress of 1000 times, the variation of breakdown field ($\%\Delta E_{1\,mA/cm^2}$) after applying the surge-current was almost −8% for the samples added with 0.25 mol% Er_2O_3 and was almost −3% for the samples added with 0.5 mol% Er_2O_3. Therefore, the samples added with 0.5 mol% Er_2O_3 exhibited the most stable $E_{1\,mA/cm^2}$ characteristics against a surge-current stress. After applying the surge stress of 1000 times, the variation of nonlinear coefficient ($\%\Delta\alpha$) was −11% for the samples added with 0.25 mol% Er_2O_3 and was almost −21% for the samples added with 0.5 mol% Er_2O_3. Therefore, the

Table 1
Breakdown field ($E_{1\,mA/cm^2}$), nonlinear coefficient (α), breakdown voltage ($V_{1\,mA}$), clamping voltage (V_c), and clamp voltage ratio (*K*) of the samples for different amounts of Er_2O_3.

Er_2O_3 amount (mol%)	$E_{1\,mA/cm^2}$ (V/cm)	α	$V_{1\,mA}$ (V)	V_c (V)					*K*				
				I_p (A)					I_p (A)				
				1	5	10	20	40	1	5	10	20	40
0.25	4026	36	421	675	765	810	850	900	1.60	1.81	1.92	2.02	2.13
0.5	4901	43	509	770	880	925	960	1020	1.51	1.73	1.82	1.89	2.0
1.0	6043	48	625	945	1060	1105	1170	1240	1.51	1.70	1.77	1.87	1.98

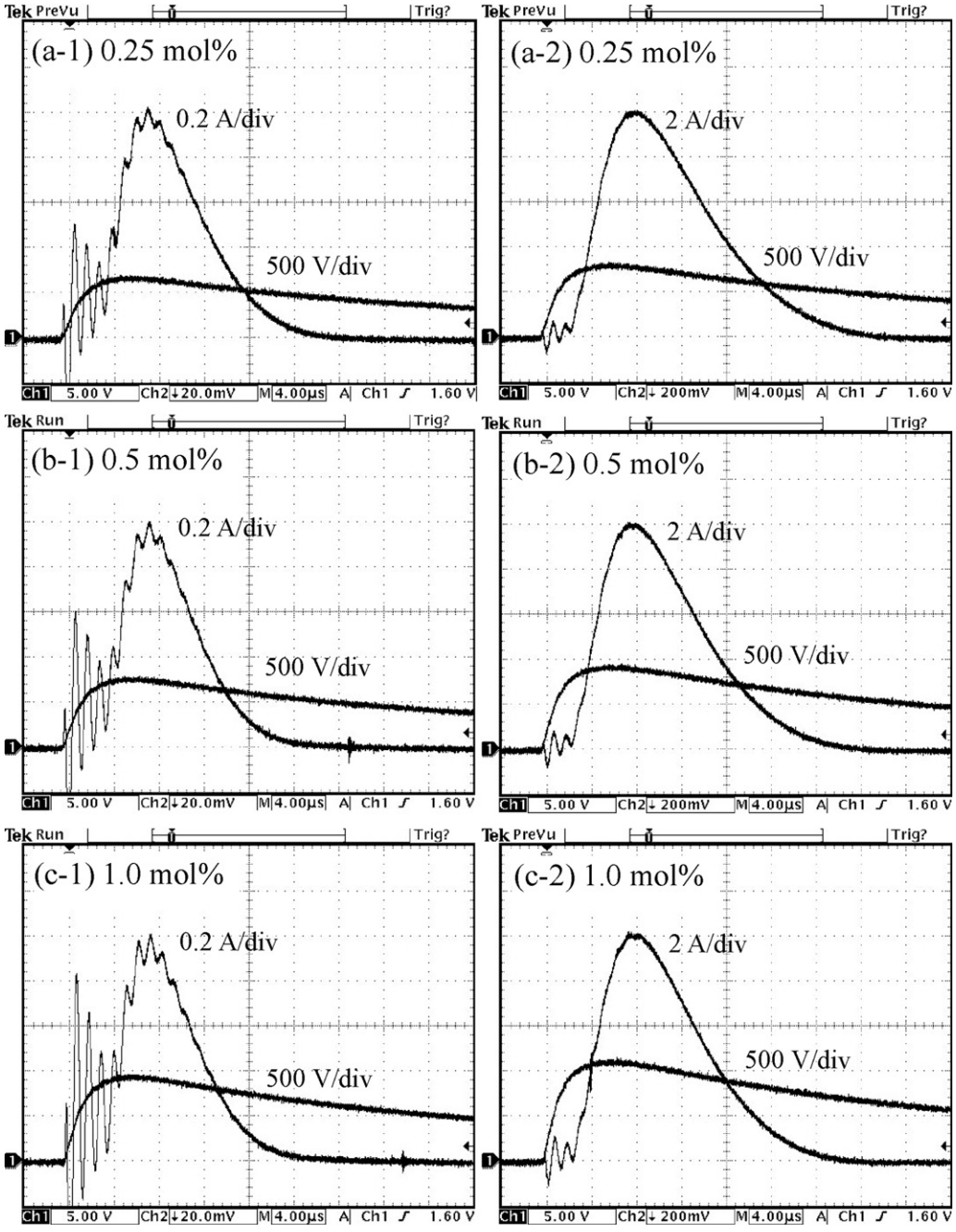

Fig. 4. Clamp voltage characteristics for 1 and 10 A surge-current of the samples for different amounts of Er_2O_3.

samples added with 0.25 mol% Er_2O_3 exhibited the most stable α characteristics against a surge-current stress. On the other hand, after applying the surge stress of 1000 times, the variation of leakage ($\%\Delta J_L$) was -72% for the samples added with 0.25 mol% Er_2O_3 and was almost -40% for the samples added with 0.5 mol% Er_2O_3. The behavior of leakage current was entirely different from the behavior of breakdown and nonlinear coefficient. In general, the varistors are degraded when it was subjected to the stress. As a result, the breakdown field and nonlinear coefficient are decreased and the leakage current is increased. However, it was found that the leakage current is decreased for specified impulse current stress [22,23] unless the varistors are abruptly degraded, unlike DC accelerated aging stress. This result may be doubtful, however the same result was obtained through several experiments. The majority of Pr_6O_{11}-based ZnO varistors exhibited the same result (the decrease of leakage current) for a surge stress. At present, the reason is not clear yet. Micro-varistor has a microstructure such as ZnO semiconductor–insulator (containing depletion layer)–ZnO semiconductor. When the low external bias is applied to both terminals of the varistor, the leakage current consisted of the thermionic emission current over the Schottky barrier, and the electron–hole recombination current and the electron trap recombination current within the depletion region. It is

Table 2
Variations of breakdown field ($E_{1\,mA/cm^2}$), nonlinear coefficient (α), and current density (J_L) with the number of applied surge-current of 100 A/cm^2 for different amounts of Er_2O_3.

Er_2O_3 amount (mol%)	Number of surge stress (100 A/cm^2)	$E_{1\,mA/cm^2}$ (V/cm)	$\%\Delta E_{1\,mA/cm^2}$	α	$\%\Delta\alpha$	J_L (μA/cm^2)	$\%\Delta J_L$
0.25	Initial	4026	–	36	–	0.7	–
	100	3758	−6.6	31	−13.9	0.21	−70.0
	400	3701	−8.1	31	−13.9	0.18	−74.3
	700	3699	−8.1	32	−11.1	0.17	−75.7
	1000	3699	−8.1	32	−11.1	0.18	−72.3
0.5	Initial	4901	–	43	–	1.5	–
	100	4796	−2.1	36	−16.2	1.0	−33.3
	400	4776	−2.5	35	−18.6	0.9	−40.0
	700	4759	−3.0	34	−20.9	0.9	−40.0
	1000	4744	−3.2	34	−20.9	0.9	−40.0
1.0	Initial	6043	–	48	–	0.8	–
	55	Failure					

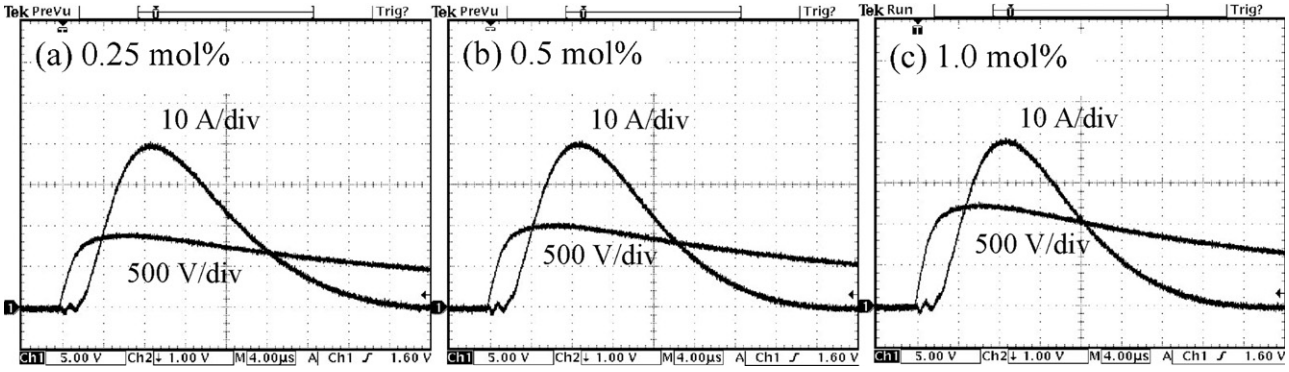

Fig. 5. Clamping voltage waveforms for surge-current (100 A/cm^2) applied to the samples for different amounts of Er_2O_3.

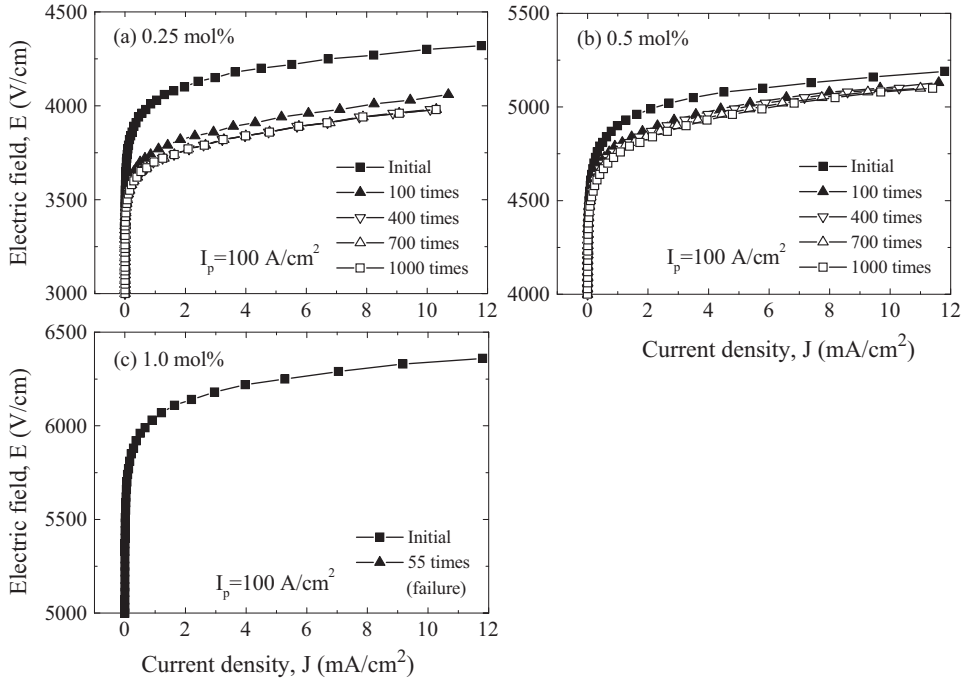

Fig. 6. *E–J* characteristics before and after applying the surge-current stress of the samples for different amounts of Er_2O_3.

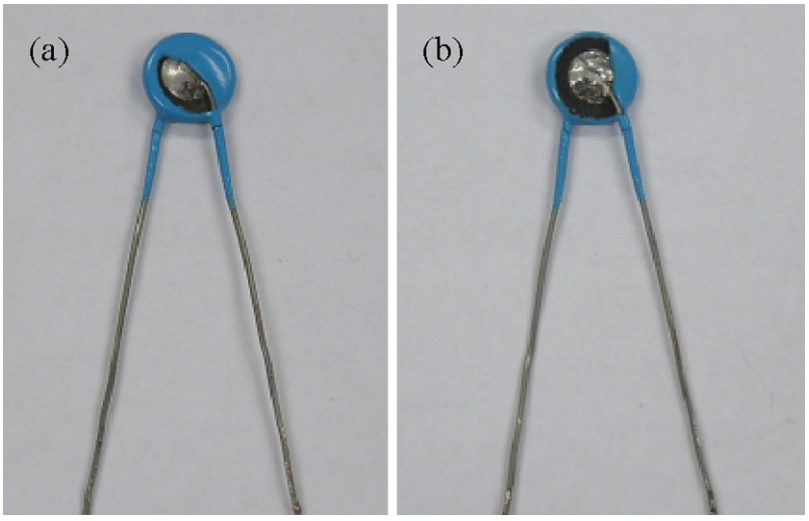

Fig. 7. Photographs of the samples destroyed by the shock of surge: (a) 1.0 mol% and (b) 0.25 mol%.

presumed that this phenomenon may be attributed to the decrease of recombination current at the grain boundaries. Forthcoming, it should be deeply studied.

Fig. 8 shows the clamping voltage waveforms for a surge-current of 400 A to compare the stability for samples added with 0.25 and 0.5 mol% Er_2O_3. The samples added with 0.25 mol% Er_2O_3 were destroyed at a surge-current of 400 A and the sample destroyed is shown in Fig. 7(b). The samples added with 1.0 mol% Er_2O_3 were destroyed after applying 55 times for a surge-current of 100 A/cm^2, as mentioned in Fig. 6. However, the samples added with 0.5 mol% Er_2O_3 were clamped at V_c = 1150 V for a surge-current of 400 A.

Fig. 9 shows the variation of E–J characteristics after applying the higher surge-current of 400 and 900 A for the

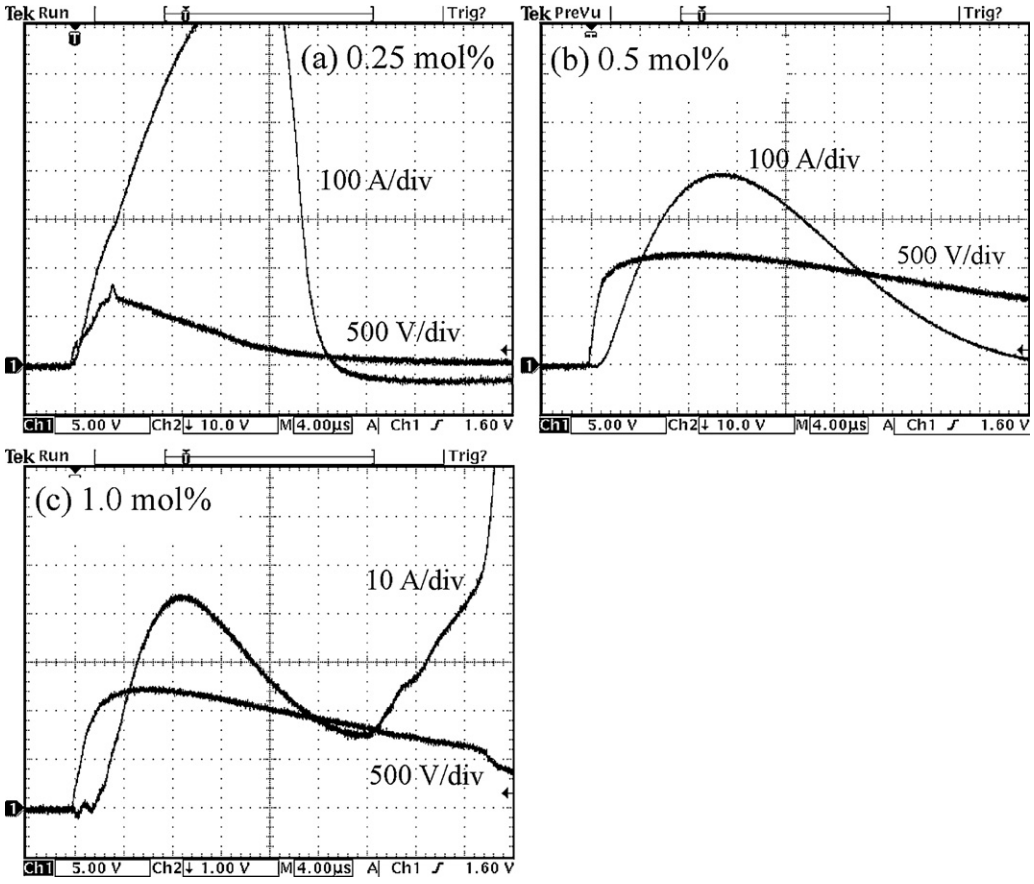

Fig. 8. Clamping voltage waveforms for surge-current (400 A) applied to the samples for different amounts of Er_2O_3.

Table 3
Variations of breakdown field ($E_{1\,mA/cm^2}$), nonlinear coefficient (α), and current density (J_L) before and after applying the surge-current of 400 A for different amounts of Er_2O_3.

Er_2O_3 amount (mol%)	Surge-current (A)	$E_{1\,mA/cm^2}$ (V/cm)	$\%\Delta E_{1\,mA/cm^2}$	α	$\%\Delta\alpha$	J_L ($\mu A/cm^2$)	$\%\Delta J_L$
0.25	Initial	4026	–	36	–	0.7	–
	400	Failure					
0.5	Initial	4901	–	43	–	1.5	–
	400	4512	−7.9	28	−34.9	0.6	−56.2
	900	3325	−32.1	12	−72.1	0.4	−73.3
1.0	Initial	6043	–	48	–	0.8	–
	100 A/cm^2	Failure					

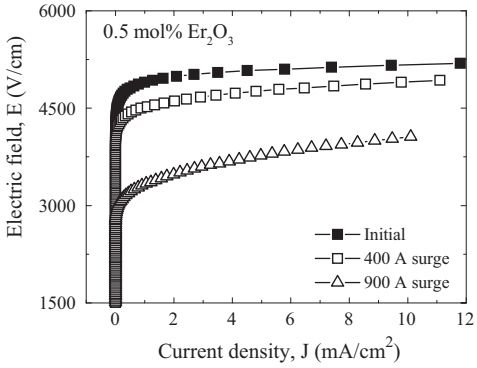

Fig. 9. *E–J* characteristics before and after applying the surge-current of the samples added with 0.5 mol% Er_2O_3.

samples added with 0.5 mol% Er_2O_3. It can be seen that the variation of *E–J* characteristics after applying the surge-current of 400 A is much larger than that after applying the surge-current of 100 A/cm^2 in Fig. 6. The samples after applying the surge-current of 400 and 900 A were abruptly degraded. After applying the surge-current of 400 A, the variation of breakdown field ($\%\Delta E_{1\,mA/cm^2}$) was almost −7.9% and the variation of nonlinear coefficient ($\%\Delta\alpha$) was −34.9%, as indicated in Table 3. However, the samples exhibited $\%\Delta E_{1\,mA/cm^2}$ less than 10% and maintained the nonlinear properties with $\alpha = 28$. Furthermore, the samples after applying the surge-current of 900 A were more greatly degraded, by exhibiting $\%\Delta E_{1\,mA/cm^2} = -32.1\%$ and $\%\Delta\alpha = -72.1\%$.

4. Conclusions

The degradation behavior against a surge-current stress in the ZPCCYE ($ZnO–Pr_6O_{11}–CoO–Cr_2O_3–Y_2O_3–Er_2O_3$) varistors was investigated for different amounts of Er_2O_3. The addition of Er_2O_3 has a significant effect on nonlinear electrical properties and surge degradation behavior of the ZPCCYE varistors. With increasing amount of Er_2O_3, the breakdown field increased from 4026 to 6043 V/cm and the nonlinear coefficient increased from 36 to 48 with increasing amount of Er_2O_3. Increasing amount of Er_2O_3 improved the clamp characteristics, in which the clamping voltage (*K*) decreases at a surge-current of 1–40 A. The varistors added with 0.5 mol% Er_2O_3 exhibited the strongest stability, with the variation rate of the breakdown field of −3.2%, the variation rate of the nonlinear coefficient of −20.9%, and the variation rate of the leakage current of −40.0% after applying 1000 times for a surge-current of 100 A/cm^2. Furthermore, the varistors added with 0.5 mol% Er_2O_3 stably absorbed a surge-current of 400 A by marking the variation rate of the breakdown field of −7.9%. On the contrary, the varistors added with 0.25 mol% were destroyed after applying the surge-current of 400 A and the varistors added with 1.0 mol% were destroyed after applying 55 times for a surge-current of 100 A/cm^2. Conclusively, proper amount of Er_2O_3 in the ZPCCYE varistors was optimized at 0.5 mol% in terms of the nonlinearity, DC accelerated aging, and surge degradation.

References

[1] C.-W. Nahm, Effect of MnO_2 addition on microstructure and electrical properties of $ZnO–V_2O_5$-based varistor ceramics, Ceram. Int. 35 (2009) 541–546.
[2] L.M. Levinson, H.R. Philipp, Zinc oxide varistor—a review, Am. Ceram. Soc. Bull. 65 (1986) 639–646.
[3] T.K. Gupta, Application of zinc oxide varistor, J. Am. Ceram. Soc. 73 (1990) 1817–1840.
[4] K. Mukae, Zinc oxide varistors with praseodymium oxide, Am. Ceram. Bull. 66 (1987) 1329–1331.
[5] K. Mukae, K. Tsuda, S. Shiga, Zinc oxide-praseodymium oxide elements for surge arresters, IEEE Trans. Power Deliv. 3 (1988) 591–598.
[6] H.K. Varma, K.P. Kumar, K.G.K. warrier, A.D. Damodaran, Effect of K_2O on the sintered microstructure of praseodymium-doped ZnO varistors, J. Mater. Sci. Lett. 8 (1989) 974–976.
[7] A.B. Alles, V.L. Burdick, The effect of liquid-phase sintering on the properties of Pr_6O_{11}-based ZnO varistors, J. Appl. Phys. 70 (1991) 6883–6890.
[8] A.B. Alles, R. Puskas, G. Callahan, V.L. Burdick, Compositional effects on the liquid-phase sintering of praseodymium oxides-based zinc oxides varistors, J. Am. Ceram. Soc. 76 (1993) 2098–2102.
[9] Y.-S. Lee, K.-S. Liao, T.-Y. Tseng, Microstructure and crystal phases of praseodymium in zinc oxide varistor ceramics, J. Am. Ceram. Soc. 79 (1996) 2379–2384.
[10] H.H. Hng, K.M. Knowles, Microstructure and current–voltage characteristics of praseodymium-doped zinc oxide varistors containing MnO_2, Sb_2O_3 and Co_3O_4, J. Mater. Sci. 37 (2002) 143–154.
[11] H. Heng, X. Fu, Z. Fu, C. Wang, L. Qi, H. Miao, Effect of TiO_2 doping on microstructure and electrical properties of $ZnO–Pr_6O_{11}$-based varistor ceramics, J. Alloys Compd. 497 (2010) 304–307.
[12] Z. Peng, X. Fu, Y. Zang, Z. Fu, C. Wang, L. Qi, H. Miao, Influence of Fe_2O_3 doping on microstructure and electrical properties of $ZnO–Pr_6O_{11}$-based varistor ceramic materials, J. Alloys Compd. 508 (2010) 494–499.
[13] C.-W. Nahm, The nonlinear properties and stability of $ZnO–Pr_6O_{11}–CoO–Cr_2O_3–Er_2O_3$ ceramic varistors, Mater. Lett. 47 (2001) 182–187.

[14] C.-W. Nahm, B.-C. Shin, Highly stable electrical properties of ZnO–Pr_6O_{11}–CoO–Cr_2O_3–Y_2O_3-based varistor ceramics, Mater. Lett. 57 (2003) 1322–1326.
[15] C.-W. Nahm, J.-A. Park, B.-C. Shin, I.-S. Kim, Electrical properties and DC-accelerated aging behavior of ZnO–Pr_6O_{11}–CoO–Cr_2O_3–Dy_2O_3-based varistor ceramics, Ceram. Int. 30 (2004) 1009–1016.
[16] C.-W. Nahm, Effect of sintering temperature on nonlinear electrical properties and stability against DC accelerated aging stress of (CoO, Cr_2O_3, La_2O_3)-doped ZnO–Pr_6O_{11}-based varistors, Mater. Lett. 60 (2006) 3311–3314.
[17] C.-W. Nahm, Electrical properties and stability of Tb-added ZnO-based nonlinear resistors, Solid State Commun. 141 (2007) 685–690.
[18] M.A. Ramírez, P.R. Bueno, W.C. Ribeiro, J.A. Varela, D.A. Bonett, J.M. Villa, M.A. Márquez, C.R. Rojo, The failure analyses on ZnO varistors used in high tension devices, J. Mater. Sci. 40 (21) (2005) 5591–5596.
[19] M.A. Ramírez, A.Z. Simoes, M.A. Márquez, Y. Maniette, A.A. Cavalheiro, J.A. Varela, Characterization of ZnO-degraded varistors used in high-tension devices, Mater. Res. Bull. 42 (2007) 1159–1168.
[20] M.A. Ramírez, A.Z. Simoes, P.R. Bueno, M.A. Márquez, M.O. Orlandi, J.A. Varela, Importance of oxygen atmosphere to recover the ZnO-based varistors properties, J. Mater. Sci. 41 (2006) 6221–6227.
[21] M.A. Ramirez, W. Bassi, P.R. Bueno, E. Longo, J.A. Varela, Comparative degradation of ZnO- and SnO_2-based polycrystalline non-ohmic devices by current pulse stress, J. Phys. D: Appl. Phys. 41 (2008) 122002.
[22] C.-W. Nahm, Electrical behavior against current impulse in ZnO–Pr_6O_{11}-based varistor ceramics with terbium addition, Ceram. Int. 36 (2010) 1495–1501.
[23] C.-W. Nahm, Al doping effect on electrical and dielectric aging behavior against impulse surge in ZPCCYA-based varistors, Mater. Sci. Eng. B 170 (2010) 123–128.
[24] C.-W. Nahm, Impulse aging behavior against of Zn–Pr–Co–Cr–Dy varistors with cobalt addition, J. Am. Ceram. Soc. 94 (2011) 328–331.
[25] C.-W. Nahm, Microstructure, electrical properties, and aging behavior of ZnO–Pr_6O_{11}–CoO–Cr_2O_3–Y_2O_3–Er_2O_3 varistor ceramics, Ceram. Int. 37 (2011) 3049–3054.
[26] J.C. Wurst, J.A. Nelson, Lineal intercept technique for measuring grain size in two-phase polycrystalline ceramics, J. Am. Ceram. Soc. 55 (1972) 109–111.